

Toy Model for Pion Production II: The role of three-particle singularities

A. Motzke^{a, b}, Ch. Elster^{a, c}, and C. Hanhart^a

^a*Institut für Kernphysik, Forschungszentrum Jülich, D-52428 Jülich, Germany*

^b*Lehrstuhl für Theoretische Chemie, Technische Universität München, D-85747 Garching,
Germany*

^c*Department of Physics and Astronomy, Ohio University, Athens, OH 45701, USA*

(November 12, 2018)

Abstract

The influence of three-particle breakup singularities on s -wave meson production in nucleon-nucleon collisions is studied within the distorted wave Born approximation. This study is based on a simple scalar model for the two-nucleon interaction and the production mechanism. An algorithm for the exact numerical treatment of the inherent three-body cuts, together with its straightforward implementation is presented. It is also shown that two often-used approximations to avoid the calculation of the three-body breakup are not justified. The possible impact on pion production observables is discussed.

PACS number(s): 25.40Qa, 13.60Le

I. INTRODUCTION

Interest in studies of pion production in nucleon-nucleon collisions at energies near the pion production threshold has been revitalized by the appearance of excellent high quality data [1]. In addition, experimental data for double polarization observables for the reactions $pp \rightarrow pp\pi^0$ [2], $pp \rightarrow pn\pi^+$ [3], and $pp \rightarrow d\pi^+$ [4] are available. A comparison of the experimental information with the predictions of a modern meson exchange model [5] shows that the data for the production of charged pions are well reproduced, whereas there are large discrepancies between the predictions and the data when considering neutral pion production. Thus, although the process of pion production has been investigated over several decades, the phenomenology of this fundamental process is still not fully resolved.

A priori one could assume that the most rigorous approach to pion production in nucleon-nucleon collisions is a complete description of the nucleon-nucleon-pion system, e.g. via coupled channel equations, as developed recently in Ref. [6]. However, not only is such a procedure difficult to implement, arguments based on effective field theories suggest that, at least close to the production threshold, most of the diagrams generated within a coupled channel approach are suppressed [7,8]. Those arguments indicate that the only piece that needs to be treated non-perturbatively is the nucleon-nucleon (NN) interaction, whereas the transition amplitude $NN \rightarrow NN\pi$ can be treated perturbatively. In this spirit, most of the recent calculations for pion production in NN collisions are based on the distorted wave Born approximation (DWBA) ¹.

Above the pion production threshold, where a virtual pion exchange can produce a real pion, one encounters a final state containing three real particles and therefore has to consider a full three-body breakup amplitude. This amplitude contains branch cut singularities. Since the evaluation of those so-called three-body singularities is technically rather involved, they have been avoided so far in all calculations that apply DWBA to meson production in NN collisions [11]. Instead, the energy-dependence of the pion propagator was manipulated in such a way that no singularity occurred. These approximations, however, were never tested quantitatively. Moreover, since the imaginary part arising from the three-body singularities scales with the three-body phase space, a strongly energy-dependent phase motion of all those amplitudes with a significant contribution from pion exchange should be expected. One might speculate that the insufficient treatment of the three-body character of the pion production may be a source of the insufficient description of the polarization data for neutral pion production mentioned before.

Recently a simple, scalar ‘toy’ model for pion production was proposed in order to investigate the validity of several approximations used with respect to the energy dependence in the pion propagator as well as in the πN amplitude [12]. Although the model used in Ref. [12] is simple with respect to the interactions, the pion dynamics is treated exactly. A significant finding of that work was that a proper treatment of the dynamics is very important, even exactly at the pion production threshold. Therefore, this model is a natural

¹Note: Even before using chiral perturbation theory, DWBA was used for calculations of the process $NN \rightarrow NN\pi$ [10]. In these calculations the only justification for this procedure was based on the slow growth of the NN inelasticities.

choice for studying the impact of an exact treatment of the three-body dynamics in the pion production process. In this work we specifically want to address the role of three-body singularities in reactions of the type $NN \rightarrow NN\pi$, and to study their possible effect on observables. In addition, we present an algorithm for their evaluation that can be implemented quite easily. For this specific study an exact treatment of the NN interaction is not necessary. The inclusion of a full NN interaction will add to the computational complexity by requiring careful interpolations of the half off-shell NN transition amplitudes, but will have no impact on the technical peculiarities induced by the three-particle singularities of the pion propagator. Such a model is thus the ideal starting point for our investigation.

This article is structured as follows: In Section II we briefly summarize the most important features of the model from Ref. [12]; in Section III the algorithm for the exact numerical evaluation of the three-body breakup singularity is given; in Section IV we present our numerical results; and we conclude in Section V.

II. THE ‘TOY’ MODEL FOR PION PRODUCTION IN NN COLLISIONS

Here the most important features of the scalar model for the production of pions in NN collisions as introduced in Ref. [12] are summarized and discussed. The main features of this model are:

i) The pion is represented by a scalar–isoscalar Klein–Gordon field that couples via a Yukawa coupling to the nucleons. Only the emission of this particle is considered.

ii) The nucleons are treated as distinguishable. As a consequence, pion emission needs to be considered only from one nucleon. The symmetric term wherein the pion is emitted from the other nucleon is omitted. The simplicity of the model is retained by allowing the pion to couple to only one of the nucleons. Therefore pion exchange between two nucleons is not contained in the model.

iii) Only pion rescattering by one nucleon is considered. This pion rescattering is described by a πN seagull vertex which is inspired by the chiral πN interaction Lagrangian.

iv) The nuclear interaction is modeled by the exchange of a heavy scalar–isoscalar Klein–Gordon field, named σ , which couples to the nucleons via Yukawa coupling. Since the strength of this coupling does not influence the three-body dynamics of the pion production process, only small couplings are considered for the one- σ exchange.

It is typical to treat pion production near threshold using a non-relativistic expansion in the nucleon momenta. In the following only leading terms in this expansion will be considered; in particular, contributions from anti-nucleons are ignored.

In summary, we consider a scalar model defined by the following Lagrangian:

$$\begin{aligned} \mathcal{L} = \sum_{j=1,2} N_j^\dagger (i\partial_0 + \frac{\nabla^2}{2M_N}) N_j + \frac{1}{2} [(\partial_\mu \pi)^2 - m_\pi^2 \pi^2 + (\partial_\mu \sigma)^2 - m_\sigma^2 \sigma^2] \\ + \frac{g_\pi}{f_\pi} N_2^\dagger N_2 \pi + g_\sigma \sum_{j=1,2} N_j^\dagger N_j \sigma + \frac{C}{f_\pi^2} N_1^\dagger N_1 (\partial_0 \pi)^2. \end{aligned} \quad (2.1)$$

Here M_N represents the physical nucleon mass of 939 MeV and m_π is 139 MeV. The mass of the σ meson is chosen to be 550 MeV. All diagrams are evaluated at order $\frac{g_\pi}{f_\pi} g_\sigma^2 \frac{C}{f_\pi^2}$. In

the following we do not display these factors, nor other constants that are common to all amplitudes. All the loops are finite, so that we do not need to introduce any regulators.

It is important to point out some of the unrealistic features of the model introduced above, even so they will not influence our study of the three-body dynamics of the pion production process. We are concerned with near-threshold kinematics, so that a scalar particle is produced in an s -wave, as is the final NN pair. Angular momentum conservation requires that the initial NN pair is also in an s -wave. In a realistic case, however, where the pions are pseudoscalar mesons, the production of s -wave pions calls for a p -wave in the initial state. Furthermore, the scalar model does not include a strong short-range repulsion. Thus the nucleons have stronger overlap within our model, as compared to a more realistic treatment. However, since the main focus of this work is the three-body dynamics of the production operator, a study within this model will still give valuable information. As an aside, the consideration of more realistic interactions would not introduce new conceptual aspects to the exact treatment of three-body singularities, but only increase the numerical effort.

In a DWBA calculation of threshold pion production, any tree level diagram is modified substantially by the contributions from the initial and final state interactions. We will therefore concentrate in our model calculations on those DWBA terms, in which only initial or final state NN interactions are present. We will thus ignore the rescattering diagram with DWBA contributions in *both* initial and final NN interactions, since this is a two-loop integration term. Again, the initial and final state interactions, which occur before or after the pion rescattering process, are represented by a single σ exchange. All diagrams are evaluated in time-ordered perturbation theory (TOPT). The diagrams involving an initial state interaction are depicted in Fig. 1. In the present work we will only study ladder diagrams, which are given by the contributions labeled I1 and I2 in that figure. There are two additional types of diagrams, namely the stretched boxes (Fig. 1-I3, I4), and graphs in which a σ is exchanged in between the emission and rescattering of the virtual pion. We ignore those here. Although both groups have three-body singularities, they introduce no additional complications and are thus not relevant for the present study.

III. CALCULATION OF THE THREE-BODY BREAKUP

As mentioned at the end of the former section we will study only ladder diagrams. The corresponding diagrams are shown in Fig. 2 together with the relevant momenta. In time-ordered perturbation theory the corresponding amplitudes are proportional to

$$A^F = \int d^3p'' V_\sigma^F G_{NN}^F (G_{\pi NN}^{F,r} - G_{\pi\pi NN}^{F,b}) , \quad (3.1)$$

$$A^I = \int d^3p'' (G_{\pi NN}^{I,r} - G_{\pi\pi NN}^{I,b}) G_{NN}^I V_\sigma^I =: A^{I,r} + A^{I,b} . \quad (3.2)$$

The superscript r (b) denotes the diagrams for pion rescattering (backscattering), namely those with a pion moving forward (backward) in time, as shown in Fig. 1 I1 (I2). The individual pieces can be directly deduced from the diagram; e.g. the two propagators in Eq. (3.2) are given by

$$G_{\pi NN}^{I,r} = \left(\frac{1}{E_{tot} - E'_+ - E'' - \omega_q + i\epsilon} \right), \quad (3.3)$$

and

$$G_{\pi NN}^{I,b} = \left(\frac{1}{E_{tot} - E'_- - E'' - \omega_q - \omega_{q'} + i\epsilon} \right). \quad (3.4)$$

The relative minus sign between the two propagators in Eqs. (3.1) and (3.2) stems from the particular form of the $\pi N \rightarrow \pi N$ transition operator, namely the pion energies that appear explicitly. The evaluation of the expressions for A^F as well as $A^{I,b}$ is straightforward since they only contain two nucleon singularities, as long as total energies E_{tot} below the two-pion threshold are considered (c.f. Eq. (3.4)). Thus in the following we will concentrate on the evaluation of the amplitude $A^{I,r}$. When discussing the results, however, the complete amplitudes A^F and as A^I will be considered.

For completeness we will also give explicitly the expressions for the other parts of $A^{I,r}$, namely the two-nucleon propagator

$$G_{NN}^I = \frac{1}{E_{tot} - 2E'' + i\epsilon}, \quad (3.5)$$

and the σ -exchange potential

$$V_\sigma^I = \frac{1}{\omega_\sigma(E_{tot} - E - E'' - \omega_\sigma)}. \quad (3.6)$$

In a model based on a realistic NN interaction, the potential V_σ^I will have to be replaced by a NN t-matrix.

The integration variable p'' in Eq. (3.2) stands for the relative momentum of the nucleons in the intermediate state. The quantity $E'_\pm = \frac{1}{2M_N}(\vec{p}' \pm \frac{\vec{q}'}{2})^2$ is the energy of the right (+) and the left (-) nucleon in the final state, $\omega_{q'} = \sqrt{m_\pi^2 + \vec{q}'^2}$ is the energy of the produced pion, and the total energy is given by $E_{tot} = 2E = E'_+ + E'_- + \omega_{q'}$. In addition, $\omega_q = \sqrt{m_\pi^2 + \vec{q}^2}$ and $\omega_\sigma = \sqrt{m_\sigma^2 + \vec{k}^2}$ denote the on-shell energies of the π and σ meson, and $E'' = \frac{\vec{p}''^2}{2M_N}$ is the energy of a nucleon in an intermediate state. The momenta \vec{q} and \vec{k} are defined through $\vec{q} = \vec{p}' + \frac{\vec{q}'}{2} - \vec{p}''$ and $\vec{k} = \vec{p} - \vec{p}''$. The momentum of the initial nucleon is labeled \vec{p} (c.f. Fig. 2).

The amplitude given by Eq. (3.2) exhibits a distinct singularity structure; it contains both, a two- and a three-body cut. Those cuts occur whenever it is energetically allowed for two or three particles in the intermediate state to go on-shell simultaneously. It should be noted that the two and three-body singularities are kinematically well separated, as shown in detail in Appendix A; whenever the intermediate two-nucleon state is on-shell, the πNN propagator is strictly negative. The numerical treatment of two-body singularities, e.g. by subtraction methods, is a well-established procedure [13]. Calculations of the three-body breakup have long history in neutron-deuteron scattering (e.g. [14–16]). In the context of NN potentials that incorporate pion production explicitly, the breakup has been treated either by complex contour deformation [17], spline methods [18], or subtraction methods

[19,20]. For the explicit calculation of pion production observables the last seem preferable, since all calculations are carried out along the real axis. For our purpose, namely the framework of DWBA, the method introduced by M. Schwamb [20,21] is most suited. Thus, this algorithm is presented here together with modifications necessary for the evaluation of the loop given in Fig. 2.

In order to proceed, the πNN propagator introduced in Eq. (3.3) is rewritten as

$$G_{\pi NN}^{I,r} = \left(\frac{E_{tot} - E'_+ - E'' + \omega_q}{2P'p''} \right) \frac{1}{x'' - x_0 + i\epsilon}. \quad (3.7)$$

Here $\vec{P}' = \vec{p}' + \frac{\vec{q}'}{2}$ and

$$\omega_q = \sqrt{m_\pi^2 + P'^2 + p''^2 - 2P'p''x''}, \quad (3.8)$$

where $x'' = (\vec{P}' \cdot \vec{p}'')/(P'p'')$. The quantity x_0 is defined as

$$x_0 \equiv x_0(P', p'') = \frac{m_\pi^2 + P'^2 + p''^2 - (E_{tot} - E'_+ - E'')^2}{2P'p''}. \quad (3.9)$$

The integration over the angle variable x'' contains a singularity for all p'' that leads to $|x_0| \leq 1$. Thus,

$$x_0 = \pm 1 \Leftrightarrow m_\pi^2 + (P' \mp p'')^2 - \left(E_{tot} - \frac{P'^2}{2M_N} - \frac{p''^2}{2M_N} \right)^2 = 0 \quad (3.10)$$

represent two conditions for the boundaries of the area containing three-particle singularities. These are two polynomial equations of degree four for $p'' = p''(P')$. Only three of the eight solutions are physically relevant, as can be easily checked by taking the threshold limit for the solutions. They enclose the area of three-particle singularities, as illustrated in Fig. 3, for a total energy of $E_{tot} = 210$ MeV. In what follows we will denote the boundaries of this area by p_a and p_b , respectively, as indicated in the figure.

Introducing the auxiliary function

$$F(x'') := (E_{tot} - E'_+ - E'' + \omega_q) \int_0^{2\pi} d\varphi'' V_\sigma^I \quad (3.11)$$

allows to rewrite the amplitude $A^{I,r}$ from Eq. (3.2) as

$$A^{I,r} = A_{3b}^I + A_{no}^I + A_{2b}^I, \quad (3.12)$$

where

$$A_\alpha^I = \frac{M_N}{2P'} \int_{R_\alpha} dp'' \frac{p''}{p^2 - p''^2 + i\epsilon} \int_{-1}^1 dx'' \frac{F(x'')}{x'' - x_0 + i\epsilon}. \quad (3.13)$$

The regions of integration are given by

$$R_{3b} = [p_a, p_b]; \quad R_{no} = [0, p_a] \cup [p_b, p_i]; \quad R_{2b} = [p_i, \infty]. \quad (3.14)$$

Here p_i denotes an in-principle arbitrary momentum placed in the interval between the region of three-body singularities and the two-nucleon singularity (c.f. Fig. 3). For the numerical evaluation we chose p_i such that it cuts this interval in half.

The term A_{3b}^I is thus the piece of the amplitude that contains the three-body cut. The second term A_{2b}^I in Eq. (3.12) stands for the remaining integration from p_i to infinity and contains only the two-nucleon singularity. Since this calculation involves only a standard, single subtraction it will not be discussed in detail. The third term, A_{no}^I , contains the integration outside the region of three-body singularities for momenta smaller than p_i and will be discussed in detail at the end of this section.

We begin our discussion with the term A_{3b}^I . For each value of x_0 we subtract and add the value of A_{3b}^I at the singularity and get

$$A_{3b}^I = \frac{M_N}{2P'} \int_{p_a}^{p_b} dp'' \frac{p''}{p^2 - p''^2} \times \left[\int_{-1}^1 dx'' \frac{F(x'') - F(x_0)}{x'' - x_0} + F(x_0) \left(\ln \left| \frac{1 - x_0}{1 + x_0} \right| - i\pi \right) \right]. \quad (3.15)$$

The complication specific to three-body singularities is the appearance of removable logarithmic singularities: the arguments of the logarithm vanish at the integration limits p_a and p_b , where $|x_0| = 1$.

The last piece of Eq. (3.15) is the imaginary part mentioned in the introduction. It leads to an additional imaginary contribution, which is necessarily energy-dependent.

Let us concentrate now on the logarithm in the last term of Eq. (3.15). Here we employ a transformation first introduced by Schwamb [21] that allows to carry out the integrals numerically in a quite straightforward fashion. In order to apply the transformation the range of integration over p'' is split into two pieces, so that there is only one singularity in each of the two intervals. The intermediate momentum is chosen to be $p_{ab} := \frac{1}{2}(p_a + p_b)$, in accordance with Ref. [21]. Using the abbreviations $\alpha(p'')$ and $\beta(p'')$, we are now faced with integrals of the type

$$\mathcal{I} := \int_{p_{ab}}^{p_b} dp'' \alpha(p'') \ln[\beta(p'')] \quad (3.16)$$

where $\beta(p_b) = 0$. The substitution

$$y^2 := p_b - p'' \geq 0 \quad (3.17)$$

allows to transform the integral of Eq. (3.16) into

$$\mathcal{I} = 2 \int_0^{\sqrt{\frac{p_b - p_a}{2}}} dy y \alpha(p_b - y^2) \ln[\beta(p_b - y^2)]. \quad (3.18)$$

Due to the minus sign in Eq. (3.17) the lower integration limit 0 is now the ‘critical’ point of the integrand. The additional factor y in Eq. (3.18) is responsible for the ‘disappearance’ of the logarithmic singularity; the integral is now regular, since $\lim_{y \rightarrow 0} y \ln(y) = 0$. The integration interval $[p_a, p_{ab}]$ is treated in a similar fashion, as described in Appendix B.

In principle, the application of a subtraction in the intervals $[0, p_a]$ and $[p_b, p_i]$ is not necessary, since singularities occur at the boundaries only. However, numerical tests showed

that applying a subtraction in these intervals also allows a smaller number of grid points in obtaining a stable and convergent result. In summary, with the above algebraic transformations, the second term in Eq. (3.12) is expressed as

$$A_{no}^I = \frac{M_N}{2P'} \int_{R_{no}} dp'' \frac{p''}{p^2 - p''^2} \times \left[\int_{-1}^1 dx'' \frac{F(x'') - F(\text{sign } x_0)}{x'' - x_0} + F(\text{sign } x_0) \ln \left| \frac{1 - x_0}{1 + x_0} \right| \right], \quad (3.19)$$

where the integration interval R_{no} was defined in Eq. (3.14).

Note that, through the splitting into intervals of the p'' integration the first term in Eqs. (3.15) and (3.19) also appears as integrated in intervals. In principle there are no numerical difficulties with this integral, however one needs to make sure that there is a sufficient number of mesh points within the region of the three-body singularities in order to obtain accurate results. That is why we propose to use the splitting of the intervals here as well. A complete presentation of the three-body cut algorithm is given in Appendix B.

IV. EFFECT OF THE THREE-BODY BREAKUP ON THE PRODUCTION CROSS SECTION

Since the ingredients of our model are of scalar nature, the only observables to be considered here are cross sections. The total cross section σ_{tot} for pion production is calculated from the coherent sum of the production amplitudes A^F and A^I defined in Eqs. (3.1) and (3.2), respectively. Here we will use the notation

$$\sigma_{tot} = \int d\rho |A^I + A^F|^2 \quad ; \quad \sigma_{tot}^F = \int d\rho |A^F|^2 \quad ; \quad \sigma_{tot}^I = \int d\rho |A^I|^2 \quad , \quad (4.1)$$

where $d\rho$ denotes the phase space factor. As a measure of the total energy we introduce the excess energy $Q = E_{tot} - m_\pi$. In the present work we concentrate on excess energies between the one-pion and two-pion threshold. Thus, if the excess energy is given in units of m_π , we restrict ourselves to values of Q/m_π between 0 and 1. In the upper panel of Fig. 4 we display the result of the full calculation, σ_{tot} (solid line), with cross sections σ_{tot}^I (dashed line) and σ_{tot}^F (dotted line) obtained from the initial and final state interactions individually.

In order to emphasize better the contributions of the FSI and ISI separately, we divide σ_{tot}^I and σ_{tot}^F by σ_{tot} and display those ratios in the lower panel of Fig. 4. The figure shows that σ_{tot}^I gives the largest contribution over the entire energy interval under consideration, while σ_{tot}^F is always close to σ_{tot} .

Naturally these features are specific to the model. More interesting is to compare the exact calculation with approximations for the pion propagator to avoid the appearance of the three-body singularities, since a main goal of this work is to investigate the quality of those approximations. Here we consider two of these approximations. In both, the πNN propagator Eq. (3.3) is substituted by a propagator containing no three-body singularity. In case of the *static approximation* (used, e.g., in Ref. [22]) the substitution

$$\frac{1}{E_{tot} - E'_+ - E'' - \omega_q + i\epsilon} \longrightarrow -\frac{1}{\omega_q} \quad (4.2)$$

is made; i.e., the π -exchange is made instantaneous. In case of the ‘*threshold approximation*’ (used in Refs. [9,23]), the πNN propagator is given by

$$\frac{1}{E_{tot} - E'_+ - E'' - \omega_q + i\epsilon} \longrightarrow \frac{1}{m_\pi - E'_+ - E'' - \omega_q}. \quad (4.3)$$

By definition, exactly at threshold this ‘threshold approximation’ agrees with the exact propagator, since the total energy E_{tot} is then equal to m_π . In the literature other approximations can be found. For example, in Ref. [7] a propagator similar to that of Eq. (4.3) is used, but with $E'_+ \equiv m_\pi/2$ and $E'' \equiv 0$. Recognizing that our list is not complete, we nevertheless consider the ‘static approximation’ and the ‘threshold approximation’ as representative and concentrate on these.

In Fig. 5 the ratios of the calculations based on the two approximations and the exactly calculated cross sections are displayed. In panel (c) of Fig. 5 the results of the full calculations (i.e. containing FSI and ISI) are shown. The dashed line gives the result for the ‘static approximation’, while the dotted line represents the ‘threshold approximation’. The figure indicates that, although the ‘threshold approximation’ is by definition exact at threshold, its energy behavior does not correspond to the exact calculation at higher energies. Especially when approaching the two-pion threshold, this approximation underestimates the full result considerably. The ‘static approximation’ overestimates the full result in the entire energy regime between the one-pion and two-pion thresholds. This is especially pronounced near the one-pion threshold. In order to investigate the effects of the approximations in more detail we display their effects calculated with FSI and ISI only in panels (a) and (b) of Fig. 5. Comparing the panels (a) and (b) with the complete calculation (c) shows that the last is the result of interference effects: due to their singularity structure A^I and A^F have different phases with different energy-dependence that are taken into account in different ways by the two approximations.

In order to study this point in more detail let us now consider the phase motion introduced by the exact inclusion of the three-body singularities. Obviously, in order to obtain a quantitative understanding, we need to compare the full result to one in which the breakup does not occur. For this comparison we choose the ‘static approximation’, defined in Eq. (4.2). In Fig. 6 we compare the phase $\phi[A]$ of the amplitudes, defined through

$$\tan(\phi[A]) = \frac{\text{Im}(A)}{\text{Re}(A)}, \quad (4.4)$$

for a fixed total excess energy $Q = \frac{1}{2}m_\pi$ as a function of the kinetic energy of the relative motion of the outgoing two nucleon system. The solid line shows the phase of the full result, while the dashed line corresponds to the ‘static approximation’. panel (a) contains the phase $\phi[A^F]$, panel (b) the phase $\phi[A^I]$, and the phase of the full calculation, $\phi[A^F + A^I]$, is shown in panel (c). As could have been expected, the phase of A^I is influenced most by the approximation, and there is a significant effect on the phase of the total amplitude. We would like to point out that for each value of Q that is smaller than m_π , the effect is qualitatively similar to the one shown in Fig. 6. Naturally, this effect is irrelevant as long as only one partial wave contributes. However, as soon as differential observables are analyzed, different partial waves start to interfere. It will be important to see how such a change in the phases of some amplitudes influences the description of the polarization data of the reaction $NN \rightarrow NN\pi$.

V. SUMMARY AND CONCLUSIONS

The effect of three-body dynamics in the pion production process within the framework of the DWBA approximation has been investigated using a scalar ‘toy’ model. This model is simple with respect to the interactions employed: the NN interaction is represented by the exchange of a scalar σ -meson; the pion is also treated as a scalar, and finally the nucleons (represented by scalar fields) are assumed to be distinguishable. However, the underlying dynamics is treated exactly, especially the three-body breakup $NN \rightarrow NN\pi$. We presented an algorithm for evaluating the three-body breakup singularities exactly. This algorithm can be applied to realistic NN interactions in a straightforward way.

Within our model we compared the results for the total production cross section with two often-used approximations: the ‘static approximation’, which makes the pion exchange instantaneous, and the ‘threshold approximation’, which fixes the total energy at the threshold value. It turns out that both approximations are different in character, but equally unsuited to describe the total pion production cross section between the one- and two-pion thresholds, at least within this model study. In case of the static approximation the cross section is overestimated over the entire energy regime, but especially close to threshold. Although the threshold approximation is exact at the threshold, it overestimates the cross section slightly close to threshold and underestimates it considerably near the two-pion threshold. Both approximations produce the wrong energy-dependence in the energy region under consideration. It remains to be seen how much of these differences survive in a realistic calculation, where, e.g., the final state interaction plays an a lot more prominent role and small momenta are suppressed due to chiral symmetry.

Finally, we compared the phases of the amplitudes of our exact calculation with the phases given by the ‘static approximation’ and found sizable differences. Although not presented in this work, a quite similar statement can be made with respect to the ‘threshold approximation’. Naturally, the phases play an important role when different partial waves interfere, as occurs for differential observables. It can then be expected that in the case of realistic interactions the description of some observables will depend crucially on the way that the three-body dynamics of the intermediate states is treated.

ACKNOWLEDGMENTS

We thank J. Durso for careful reading of the manuscript. This work was performed in part under the auspices of the U. S. Department of Energy under contract No. DE-FG02-93ER40756 with Ohio University.

APPENDIX A: LOCATION OF THE TWO AND THREE-BODY SINGULARITIES

We demonstrate here that the two- and three-body singularities from Eq. (3.2) are well separated. The two particle singularity occurs at

$$p'' = p = \sqrt{M_N E_{tot}}, \quad (\text{A1})$$

i.e., in case of on-shell scattering. An estimate for the denominator of the three-body propagator clarifies the position of its singularities, namely

$$\begin{aligned} \forall \tilde{p} \geq p: \quad & E_{tot} - E'_+ - E''(p'' = \tilde{p}) - \omega_q(p'' = \tilde{p}) \\ & \leq \frac{E_{tot}}{2} - E'_+ - \omega_q(p'' = \tilde{p}) < 0, \end{aligned} \quad (\text{A2})$$

since $E''(p'' = \tilde{p}) \geq E = \frac{E_{tot}}{2}$, and $E_{tot} < 2m_\pi$, $\omega_q \geq m_\pi$, and $E'_+ = \frac{p'^2}{2M_N} \geq 0$. Consequently the πNN -propagator is regular for all $\tilde{p} \geq p$. In particular, the position of the two-nucleon pole occurs *above* each three-particle singularity. This leads to the natural decomposition of the radial integration interval $\int_0^\infty = \int_0^{p_i} + \int_{p_i}^\infty$ (c.f. Eq. (3.12)), where $[0, p_i]$ contains all three-body singularities and $[p_i, \infty]$ contains the two-body singularity.

APPENDIX B: ANALYTIC AND NUMERIC TREATMENT OF THE LOGARITHMIC SINGULARITIES

Here we give a brief but complete presentation of the three-body cut algorithm. With

$$\xi_0 := \begin{cases} x_0 & \text{if } |x_0| \leq 1 \\ \text{sign } x_0 & \text{if } |x_0| > 1 \end{cases} \quad (\text{B1})$$

(i.e., $\xi_0 = x_0$ in $R_{3b} = [p_a, p_b]$ and $\xi_0 = \text{sign } x_0$ in $R_{no} = [0, p_a] \cup [p_b, p_i]$), the contribution $A_{3b}^I + A_{no}^I$ (c.f. Eqs. (3.12), (3.15), and (3.19)) to the production amplitude reads

$$A_{3b}^I + A_{no}^I = A^{I, \ln} + A^{I, \Delta} + i \text{Im}(A_{3b}^I), \quad (\text{B2})$$

where

$$\text{Im}(A_{3b}^I) = -\frac{\pi M_N}{2P'} \int_{p_a}^{p_b} dp'' \frac{p'' F(x_0)}{p^2 - p''^2}, \quad (\text{B3})$$

$$A^{I, \ln} := \frac{M_N}{2P'} \left(\int_0^{p_a} + \int_{p_a}^{p_{ab}} + \int_{p_{ab}}^{p_b} + \int_{p_b}^{p_i} \right) dp'' \frac{p'' F(\xi_0)}{p^2 - p''^2} \ln \left| \frac{1 - x_0}{1 + x_0} \right|, \quad (\text{B4})$$

and

$$A^{I, \Delta} := \frac{M_N}{2P'} \left(\int_0^{p_a} + \int_{p_a}^{p_b} + \int_{p_b}^{p_i} \right) dp'' \frac{p''}{p^2 - p''^2} \int_{-1}^1 dx'' \frac{F(x'') - F(\xi_0)}{x'' - x_0}. \quad (\text{B5})$$

$A^{I, \ln}$ denotes the real contribution to $A_{3b}^I + A_{no}^I$ containing the logarithm originating in the principal value of the analytically solvable integral, and $A^{I, \Delta}$ is the other real contribution originating in the application of the subtraction method. The expression $A^{I, \ln} =: \frac{M_N}{2P'} \sum_{j=1}^4 \mathcal{I}_j$ from Eq. (B4) is to be understood as if the corresponding Schwamb's substitution would have been already performed in each of the four integrals (c.f. Table I).

REFERENCES

- [1] H.O. Meyer et al., Phys. Rev. Lett. **65** (1990) 2846 and Nucl. Phys. A **539** (1992) 633.
- [2] H. O. Meyer *et al.*, Phys. Rev. C **63**, 064002 (2001).
- [3] W. W. Daehnick *et al.*, Phys. Rev. C **65** (2002) 024003
- [4] B. von Przewoski *et al.*, Phys. Rev. C **58** (1998) 1897.
- [5] C. Hanhart et al., Phys. Rev. C **61** (2000) 064008
- [6] D. R. Phillips and I. R. Afnan, Annals Phys. **247** (1996) 19; A. N. Kvinikhidze and B. Blankleider, Nucl. Phys. A **574** (1994) 788.
- [7] T.D. Cohen, J.L. Friar, G.A. Miller, and U. van Kolck, Phys. Rev. C **53**, 2661 (1996);
- [8] C. Hanhart, U. van Kolck, and G. A. Miller, Phys. Rev. Lett. **85** (2000) 2905.
- [9] C. Hanhart et al., Phys. Lett. **B358**, 21 (1995).
- [10] D. Koltun and A. Reitan, Phys.Rev. **141**, 1413 (1966).
- [11] c.f. C. Hanhart, arXiv:nucl-th/9911023, published in *Bloomington 1999, Nuclear physics at storage rings* 81-95, edited by H.-O. Meyer, P. Schwandt. Melville, AIP, 2000 and references therein.
- [12] C. Hanhart, G. A. Miller, F. Myhrer, T. Sato, and U. van Kolck, Phys. Rev. C **63** (2001) 044002.
- [13] M.I. Haftel and F. Tabakin, Nucl. Phys. **A158**, 1 (1970).
- [14] W. Glöckle, The Quantum Mechanical Few-Body Problem, Springer Verlag 1983.
- [15] H. Witala, W. Glöckle, Th. Cornelius, Few-Body Systems **3**, 301 (1988).
- [16] T. Takejami, Prog. Theor. Phys. **74**, 301 (1985).
- [17] Ch. Elster, W. Ferchländer, K. Holinde, D. Schütte, and R. Machleidt, Phys. Rev. **C37**, 1647 (1988).
- [18] A. Matsuyama and T.S.H. Lee, Phys. Rev. **C34**, 1900 (1986).
- [19] E. van Faassen and J.A. Tjon, Phys. Rev. **C33**, 2105 (1986).
- [20] M. Schwamb and H. Arenhövel, Nucl. Phys. **A690**, 647 (2001).
- [21] M. Schwamb, PhD. Thesis, U. Mainz, 2000.
- [22] B.-Y. Park, F. Myhrer, J.R. Morones, T. Meissner, and K. Kubodera, Phys. Rev. **C53**, 1519 (1996).
- [23] C. Hanhart, PhD. Thesis, U. Bonn, Jül- Rep. 3476, 1997.

TABLES

TABLE I. Schwamb's substitutions in the four parts of the interval $[0, p_i]$.

interval	transformation	contribution \mathcal{I}_i
$[0, p_a]$	$y^2 := p_a - p'' \geq 0$	$-2 \int_{\sqrt{p_a}}^0 dy y \alpha(p_a - y^2) \ln[\beta(p_a - y^2)]$
$[p_a, p_{ab}]$	$y^2 := p'' - p_a \geq 0$	$2 \int_0^{\sqrt{p_{ab}-p_a}} dy y \alpha(p_a + y^2) \ln[\beta(p_a + y^2)]$
$[p_{ab}, p_b]$	$y^2 := p_b - p'' \geq 0$	$-2 \int_{\sqrt{p_{ab}-p_a}}^0 dy y \alpha(p_b - y^2) \ln[\beta(p_b - y^2)]$
$[p_b, p_i]$	$y^2 := p'' - p_b \geq 0$	$2 \int_0^{\sqrt{p_i-p_b}} dy y \alpha(p_b + y^2) \ln[\beta(p_b + y^2)]$

FIGURES

FIG. 1. The six TOPT diagrams of the initial state interaction. A pion field is represented by a dashed line, the nucleon by a single solid line. The two possible time orderings of the σ -exchange (solid double line) lead to the identical contributions grouped in I1 and I2, for each of two ladder diagrams. I3 and I4 are stretched boxes.

FIG. 2. Feynman diagram and choice of coordinates for a) final- and b) initial-state interaction. All momenta indicated are three-momenta.

FIG. 3. The region of three-body singularities for $E_{tot}=210$ MeV and the choice of the integration intervals for the three-body cut algorithm. Inside the region enclosed by the solid line we have $|x_0| < 1$ and on the boundary $|x_0| = 1$. Additionally, the two-particle singularity at $p \simeq 444$ MeV is marked. The symbol + (-) means that the corresponding boundary curve is solution of $x_0 = +1$ ($x_0 = -1$) (c.f. Eq. (3.10)).

FIG. 4. The total production cross section as function of the excess energy, which is given in units of m_π . In the upper panel (a) the full calculation is represented by the solid line, the calculation with the FSI (ISI) only is shown as dotted (dashed) line. The lower panel (b) shows the ratios of the calculations containing the FSI (dashed) and ISI (dotted) only to the full calculation (solid line in panel (a)).

FIG. 5. The ratios of the total cross section of the static approximation (dashed curve) and the ‘threshold approximation’ (dotted curve) to the total cross section of the corresponding exact calculation. The calculations of panel (a) contain only the FSI, the calculations of panel (b) only the ISI. In panel (c) the ratios of the full calculations are shown.

FIG. 6. The phase of the production amplitude in degrees as a function of the kinetic energy of the relative motion of the NN -system (ε in units of m_π) at the excess energy $Q = \varepsilon_{max} = \frac{1}{2} m_\pi \simeq 70$ MeV. The solid lines represent the exact calculation, the dashed lines the ‘static approximation’. In panel (a) calculations with the FSI only are shown, in panel (b) those with the ISI only. The full calculations, i.e. the superposition of (a) and (b), are shown in panel (c). Qualitatively, for each Q with $0 \leq Q < m_\pi$ the illustrated dependence is the same.

Fig. 1

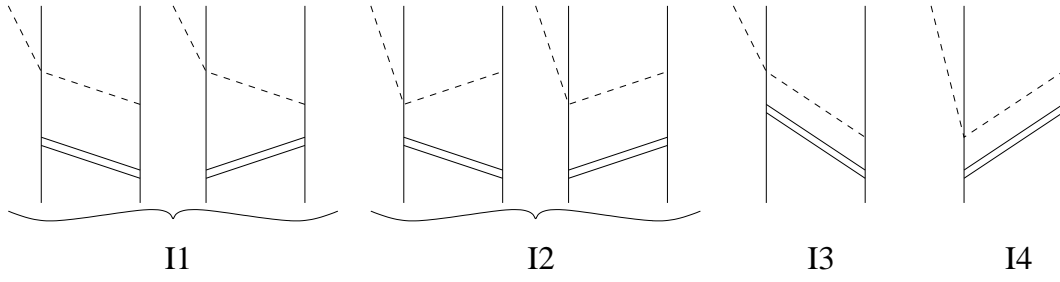


Fig. 2

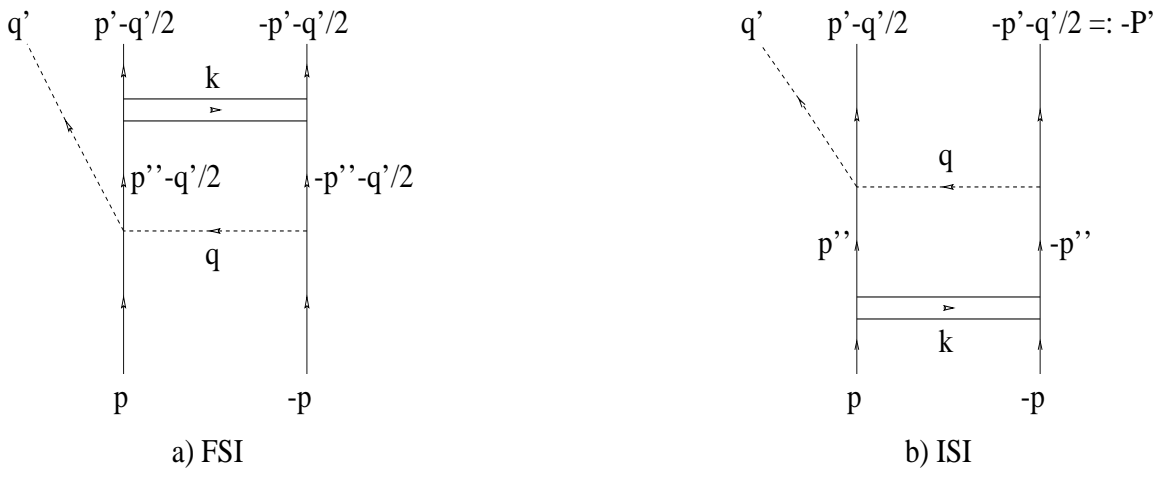


Fig. 3

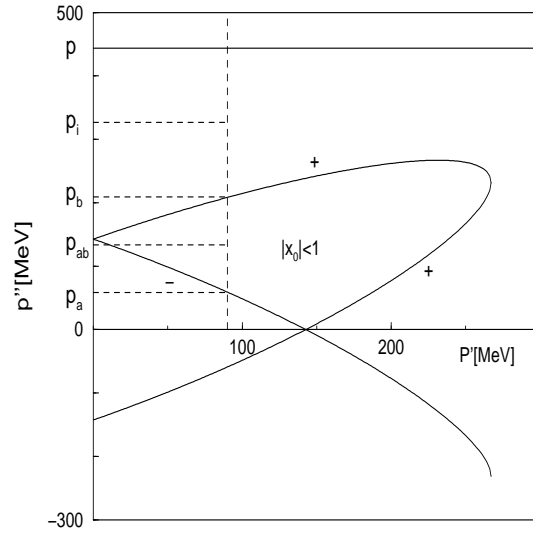


Fig. 4

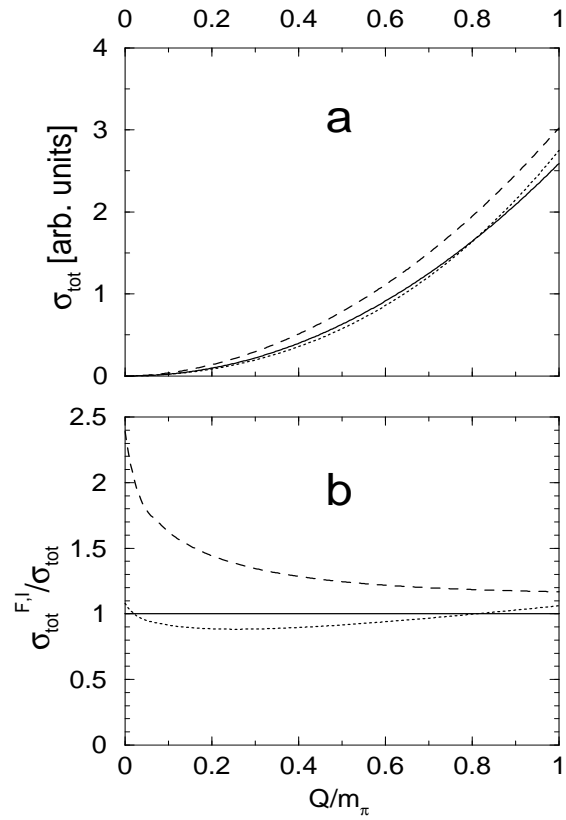


Fig. 5

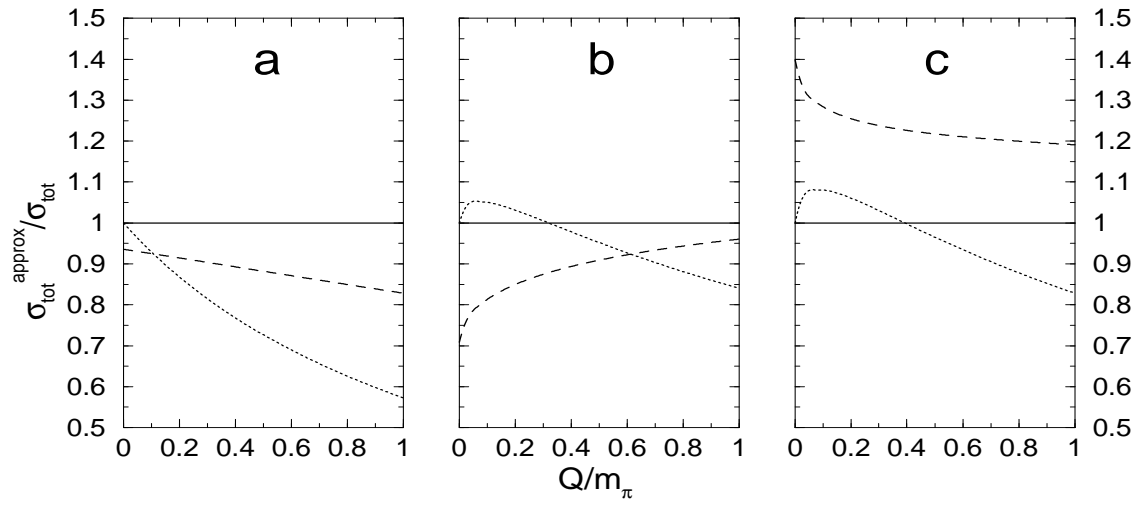


Fig. 6

